Korean J. Chem. Eng., **29**(11), 1508-1515 (2012)
DOI: 10.1007/s11814-012-0036-x

Surface recession mechanism of carbon fiber reinforced plastic layer by thermal decomposition

Jae Hun Lee*,*, Kwang Seok Kim**, and Hyo Kim***,†**

*Safety Research Division, Institute of Gas Safety R&D, Gyeonggi-do 429-712, Korea
**Korea Institute of Science and Technology (KIST), Seoul 136-791, Korea
***Department of Chemical Engineering, The University of Seoul, Seoul 130-743, Korea
(*Received 24 December 2011 • accepted 10 March 2012*)

Abstract−We tested the thermal resistance of a carbon-fiber-reinforced fuel storage tank by using the simulations and the experiments. A model describing the one-dimensional heat transfer in a composite wall exposed to a flame was developed. As a moving boundary condition, the thickness recession is expressed by the one-step Arrhenius-type decomposition kinetics. The differential equations are solved by the Crank-Nicolson method, the algorithm of which is developed by us. For the experimental verification of the simulation, the well-controlled heat is added to one side of the square specimen taken from a carbon-fiber-wounded epoxy cylinder and the change in mass of the specimen is recorded as time passes. From the comparison of the results of two methodologies, it is hypothesized that the normalized thickness by the initial value should be always equal to the normalized mass by the initial value at a certain time. As a result, the surface recession data obtained by the simulations provide good predictions for those by the experiments.

Key words: Carbon Fiber Reinforced Plastic (CFRP), Heat Transfer, Cone Calorimeter, Kinetics, Thermal Decomposition

INTRODUCTION

Since the 1980's, the fuel storage cylinders for spacecraft have been made mainly of composite materials due to their efficient storage capacity [1]. Recently, natural gas vehicles or fuel cell vehicles have also been equipped with composite cylinders for the purposes of increasing driving performances and reducing CO_2 emissions. However, the relatively low thermal resistance of polymer composite cylinders has always been a major concern among engineers. For guaranteed safety, the thickness of a cylinder wall should be determined proportional to the working pressure of the cylinder. However, continuous excessive heat received by the surface of a composite cylinder causes the disintegration of polymer resin (i.e., thickness recession) and the increased vapor pressure of the stored fuel. In addition, it is known that the mechanical strength of this composite material deteriorates when it is heated over 473 K [2].

In the case where thickness recession continues and vapor pressure exceeds the mechanical limitation of the cylinder, the vessel can break and the flammable fuel can leak. This may lead to disastrous events such as serious injuries and major property loss. Estimation of the time elapsed before the cylinder ruptures plays a key role in preventing such accidents. In this context, keen understanding of thickness recession as a function of the heat exposure time is very important. The mechanisms involved in the disaster scenarios are heat transfer by conduction, convection and radiation. Modeling and simulation studies on thermal decomposition and heat transfer through composite materials have been conducted so far by many researchers [3-9].

To set up a model to describe the extent of pyrolysis, also known as thermal degradation, one of two already-suggested hypotheses must be adopted [10]: pyrolysis takes place only at the surface of a composite and the degraded portion is immediately removed from the surface of the remaining composite material; pyrolysis takes place throughout the composite layer where the local temperature is higher than a set value (i.e., the ignition temperature), and char formed as a result of decomposition remains in place. If the former hypothesis is used, then it is necessary to measure the wall thickness of the sample cylinder in order to estimate the extent of pyrolysis. In the latter case, it is necessary to record the mass of the sample, instead. The two mechanisms are not mutually exclusive because both play an important role in weakening the mechanical strength of the cylinder. Therefore, the present study presumes that the fractional thickness (defined as the thickness of the remaining layer divided by the initial sample thickness) is identical to the fractional mass (defined as the mass of the remaining layer divided by the initial sample mass). In fact, the modeling and simulation part of the current work adopted the surface recession depth for describing the decomposed-out layer; while the data obtained through experimentation are the change in mass. In the end, the two results are properly compared.

Although the current experiments use change of mass for estimating rate of pyrolysis, the previous experiments where thickness was directly measured by observing sample cross-section with a microscope are also found: Mouritz and Mathys [11] showed that char layer thickness of glass fiber-reinforced plastics grew at a rate proportional to the square root of the heat exposition time after pyrolysis began. Gibson et al. [12] performed the experiments with three kinds of composites (glass fiber+polyester resin, glass fiber+phenolic resin, and glass fiber+vinyl resin) in the cone calorimeters to show that predictions of residual resin content (RRC) based on the one-dimensional thermal model are consistent with experimental results.

†To whom correspondence should be addressed.
E-mail: hkim@uos.ac.kr

Gardiner et al. [13] suggested the equation that relates the char layer thickness to the flexural/compressive properties. Finally, Burchill et al. [14] revealed that the char layer thickness is directly proportional to the mass ever lost during the experiment where a composite plate made of isophthalic polyester resin and E-glass fiber was burnt on a kerosene fuel tray. In this experiment, the char layer

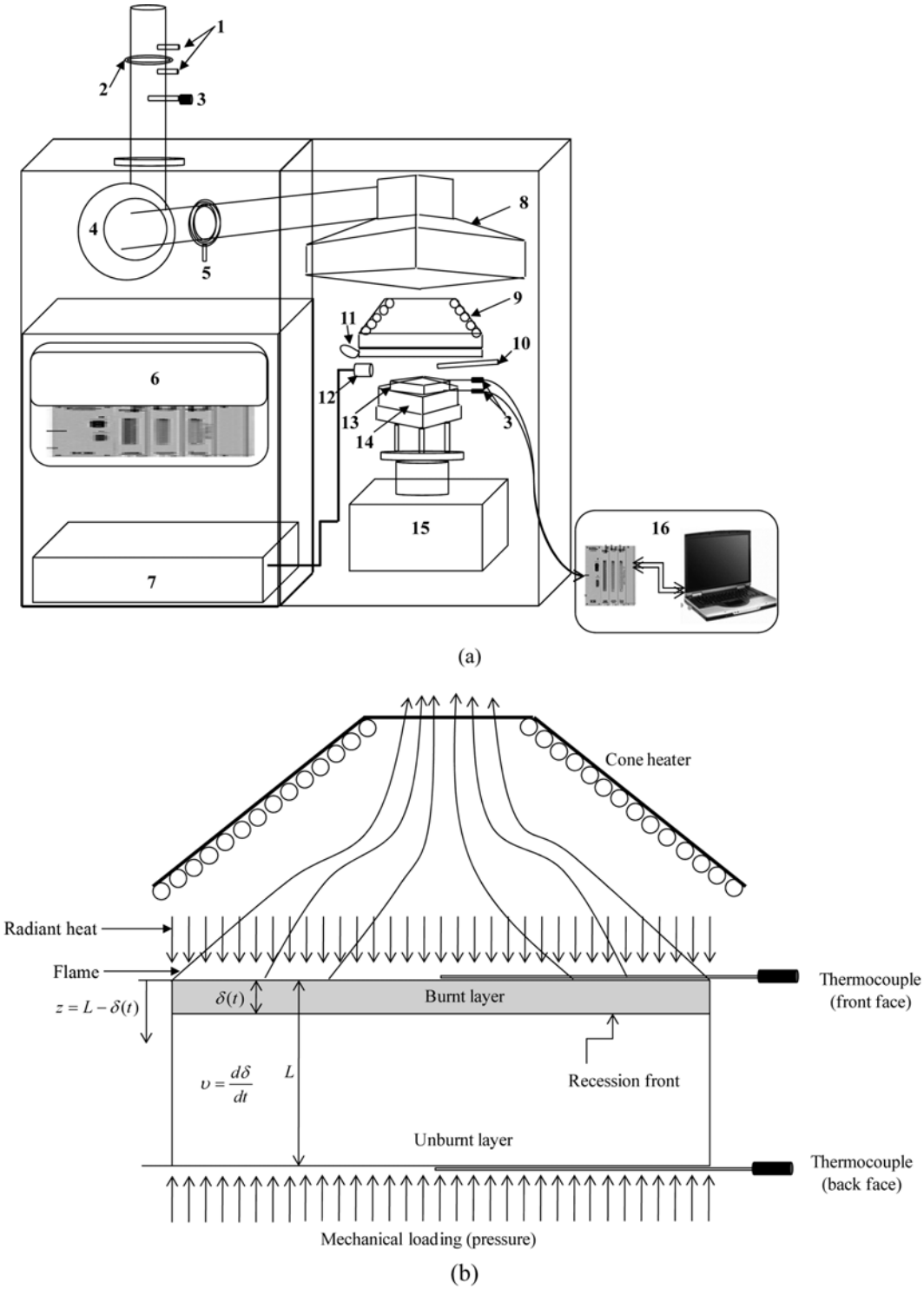

Fig. 1. (a) Perspective view of the cone calorimeter used in the experiment. (b) Schematic of the CFRP layer showing the heat transfer direction, the thermocouples and the surface recession.

1. Pressure port
2. Orifice plate
3. Thermocouple
4. Blower
5. Gas sampling prot
6. Data acquisition system (mass)
7. Water circulation system
8. Exhaust hood
9. Cone heater
10. Spark igniter
11. Shutter
12. Heat flux meter
13. Sample
14. Sample holder
15. Micro load cell
16. Data acquisition system (temperature)

thickness was measured by microscope after removing the sample from heat and cooling it. The measurements were repeated several times in the middle of the experiment.

In fact, even an observation of a sample cross-section with a microscope may not give an exact thickness because of an ambiguous boundary between burned and unburned layers. Burchill et al. [14] found a linear relation between the changes in the char layer thickness and in the mass of sample as the heating time increases. This means that the char layer thickness can be indirectly estimated by measuring mass of sample during the experiment with micro load cell-equipped fuel tray or cone calorimeter. Measuring the mass may be more efficient because it can be done without any external disturbance. The present study, a one-dimensional heat transfer through the composite layer, one surface of which is heated by radiation, has been analyzed based on the model suggested by Griffis et al. [15] and Kindelan and Liñán [16]. The model includes the effect of thermal decomposition on the heat transfer in the specimen. A one-step Arrhenius type decomposition kinetics was used to build up the equation for describing the behavior of thickness of a composite cylinder wall that is exposed to a flame. The results of the simulation are compared with the experimental data.

MATERIALS AND METHODS

1. Heat Transfer Model

In this study, we can use the Cartesian coordinates and the one-dimensional heat transfer model without the loss of accuracy, because of the large radius of curvature of the cylinder compared to the wall thickness. In addition, we can take advantage of the *infinite plate* assumption, which suggests that heat flux does not occur in lateral directions (i.e., x and y). Hence, the total heat transfer rate into the cylinder is calculated from the heat flux at the innermost surface multiplied by the surface area (i.e., $2\pi RL$). For the notation convenience, we call the surface where external heat is applied the *front face*; and the opposite surface in contact with the cylinder's fuel the *back face* (see Fig. 1). These correspond to the outermost and the innermost surfaces of the cylinder, respectively.

The origin of the Cartesian coordinates was placed at the front face, and the initial thickness of the sample was denominated as set L. As pyrolysis proceeds in the specimen, the front face moves inward. The distance from the initial surface to the burning front face is defined as the surface recession depth $\delta(t)$, and the model equation describing the temperature (T in K) distribution

$$\rho C_p \frac{\partial T}{\partial t} = \frac{\partial}{\partial z}\left(k\frac{\partial T}{\partial z}\right) + \rho C_p \upsilon \frac{\partial T}{\partial z}. \tag{1}$$

holds for the remaining layer from z=0 to z=L−δ(t). The governing equation is subject to the initial and boundary conditions such that

$$T(t=0) = T_\infty, \tag{2}$$

$$\rho H_g \upsilon = \varepsilon(q'' + q''_{fl}) - h(T_s - T_\infty) - \sigma\varepsilon(T_s^4 - T_\infty^4) + k\left.\frac{\partial T}{\partial z}\right|_{z=0}, \tag{3}$$

and

$$-k\left.\frac{\partial T}{\partial z}\right|_{z=L-\delta} = h(T_L - T_\infty) + \varepsilon\sigma(T_L^4 - T_\infty^4). \tag{4}$$

Table 1. Values of parameters and constants used in the simulation

Symbols	Value	Symbols	Value
L	0.00786	n	2
ρ	1588.39−0.0425T	E_a	329,490
C_p	685.750+1.3933T	A	7.20×10^{25}
k	0.99710−0.0008T	ε	0.6835+0.0002T
n	10 (ref. [18])	H_g	1,915,550*

*The value is calculated from the equation $H_g=C_{P0}T_{ig}^2/T_\infty$ (see ref. [19]) where C_{P0} is the heat capacity at T_∞, and T_{ig} is the ignition temperature

respectively. In the above equations, the density ρ, the heat capacity C_p and the thermal conductivity k of the composite vary with temperature. The surface recession rate υ is a function of temperature as well, and the details will be discussed later. The temperatures at the specific locations are also defined such that T_∞=25 °C, T_s=T at z=0, and T_L=T at z=L−δ(t). It is worth noticing that the radiant heat flux q″ is transferred to the specimens by an external heat source, and the burning flame heat flux q''_{fl} is generated as a result of thermal decomposition of the composite. The boundary conditions also contain the heat of decomposition H_g, the emissivity ε, the Stefan-Boltzmann constant σ is 5.676×10^{-8} W m^{-2} and the convective heat transfer coefficient h. The values of these parameters and the constants are summarized in Table 1. Note that the linear temperature dependency of the emissivity ε is assumed in the range from 293 K (ε=0.75) to 1,273 K (ε=0.95) [17].

The surface recession rate can be defined as the first derivative of the surface recession depth with respect to time:

$$\upsilon = \frac{d\delta}{dt}. \tag{5}$$

In addition, the rate of change in mass m as a result of the thermal decomposition of resin contained in the composite specimen follows the one-step Arrhenius equation,

$$\frac{dm}{dt} = -A(m_i - m_f)\left(\frac{m-m_f}{m_i-m_f}\right)^n \exp\left(-\frac{E_a}{RT_s}\right). \tag{6}$$

where A, n and E_a are the overall pre-exponential factor, the reaction order and the activation energy, respectively. The universal gas constant R is 8.314 J/mol·K. And the subscripts i and f denote the quantities at the initial and the final states, respectively.

We assume that the carbon fiber included in the composite material is not decomposed, the thermal expansion of composite material can be negligible, polymer resin can be uniformly distributed onto the composite, the thermal decomposition will take place uniformly throughout the prepared sheet, and after the experiment, no residual resin is left on the sample. The mass of the polymer resin contained in the composite material can be expressed as follows:

$$m_i = \rho a_s (L-0), \tag{7}$$

$$m = \rho a_s (L-\delta(t)), \tag{8}$$

$$m_f = 0. \tag{9}$$

Plugging Eqs. (7), (8) and (9) into Eq. (6) results in the equation

describing the surface recession rate as a function of temperature and exposition time such that

$$\frac{d\delta}{dt} = LA\left(\frac{L-\delta}{L}\right)^{n} \exp\left(-\frac{E_a}{RT_s}\right). \quad (10)$$

Eq. (10) is based on the Arrhenius-type kinetics, which was suggested and modified by Kindelan and Liñán [16].

In the present study, we also assumed that the radiational heat flux emitted from the cone calorimeter heater is constant; char formation does not change the heat transfer mechanism [10]; the heat transfer coefficient of the composite material, h, does not vary with temperature; heat conductivity, heat capacity and density of the composite are only functions of temperature; and emissivity is also only a function of temperature. The pyrolysis temperature T_p is defined as the temperature above which the resin contained in the composite material decomposes. It was measured using a thermogravimetric analyzer (TGA) in the pure N_2 environment. The TGA records the weight of the sample while it increases in temperature. In fact, the TGA data shows that the weight of a specimen begins to reduce at a very low temperature, and the reduction increases at certain higher temperatures. Pyrolysis temperature is determined on the grounds that the weight loss can also be caused by evaporated moisture that brings about decomposition. In the case of a composite material, a specimen usually loses 5% of its original weight before reaching pyrolysis temperature. It is worth noticing that heating composite materials to their pyrolysis temperature in a cone calorimeter under atmospheric environment causes volatile gas to ignite.

Both the partial differential equations and the conditions, Eqs. (1) to (5) and (10), are solved by following the Crank-Nicolson method. In the implicit method, a 3-point centered finite difference is used to approximate the first and the second derivatives. First, the N (e.g., 60) computational nodes evenly discretized the domain, $0<z<L-\delta(t)$. At the *i-th* node, the nonlinear equation, Eq. (1), is linearized by using the Taylor series expansion and is expressed in the matrix form:

$$\begin{bmatrix} a_1 & b_1 & c_1 & 0 & 0 & \cdots & 0 \\ 0 & a_2 & b_2 & c_2 & 0 & \cdots & 0 \\ \vdots & & & \ddots & & & \vdots \\ 0 & \cdots & a_i & b_i & c_i & \cdots & 0 \\ \vdots & & & & \ddots & & \vdots \\ 0 & \cdots & 0 & a_{N-1} & b_{N-1} & c_{N-1} & 0 \\ 0 & \cdots & 0 & 0 & a_N & b_N & c_N \end{bmatrix} \begin{bmatrix} T_{1,j+1} \\ \vdots \\ T_{i-1,j+1} \\ T_{i,j+1} \\ T_{i+1,j+1} \\ \vdots \\ T_{N,j+1} \end{bmatrix} = \begin{bmatrix} \Gamma_1 \\ \vdots \\ \Gamma_{i-1} \\ \Gamma_i \\ \Gamma_{i+1} \\ \vdots \\ \Gamma_N \end{bmatrix}, \quad (11)$$

where the elements of the tridiagonal matrix are defined as

$$a_i = (\lambda_1 - \lambda_2) - 2\lambda_3(T_{i+1,j+1} - T_{i-1,j+1} + T_{i+1,j} - T_{i-1,j}), \quad (12)$$

$$b_i = -2(\lambda_1 + 1), \quad (13)$$

$$c_i = (\lambda_1 + \lambda_2) + 2\lambda_3(T_{i+1,j+1} - T_{i-1,j+1} + T_{i+1,j} - T_{i-1,j}), \quad (14)$$

and,

$$\Gamma_i = (\lambda_1 - \lambda_2)\tau_{i-1} - (2\lambda_1 + 1)\tau_i + (\lambda_1 + \lambda_2)\tau_{i+1} + \lambda_3(\tau_{i+1} - \tau_{i-1} + T_{i+1,j} - T_{i-1,j})^2 + (\lambda_1 - \lambda_2)T_{i-1,j} + (1 - 2\lambda_1)T_{i,j} + (\lambda_1 + \lambda_2)T_{i+1,j} + [\lambda_1 - 2\lambda_2(T_{i+1,j+1} - T_{i-1,j+1} + T_{i+1,j} - T_{i-1,j})]\tau_{i-1} - (1 + 2\lambda_1)\tau_i + [\lambda_1 + 2\lambda_2(T_{i+1,j+1} - T_{i-1,j+1} + T_{i+1,j} - T_{i-1,j})]\tau_{i+1}, \quad (15)$$

where i=1, 2, ⋯, N. The coefficients λ_1, λ_2 and λ_3 are defined as

$$\lambda_1 = \frac{k\Delta t}{\rho C_p 2(\Delta z)^2}, \quad (16)$$

$$\lambda_2 = \frac{\upsilon \Delta t}{4\Delta z}, \quad (17)$$

$$\lambda_3 = \frac{(dk/dT)\Delta t}{16(\Delta z)^2 \rho C_p}. \quad (18)$$

The subscript j denotes quantity at t=t, and thus, j+1 stands for the quantity at t=t+Δt. The Greek letter τ is a dummy variable used for representing the intermediate temperature during the iterations.

In Eq. (15) with i=1, the values of τ_0 and $T_{0,j}$ are taken as the positive real roots of the corresponding boundary condition, Eq. (3), expressed such that

$$\tau_0^4 + \left[\frac{h}{\varepsilon\sigma} + \frac{k}{\varepsilon\sigma(\Delta z)}\right]\tau_0 - \left[\frac{k}{\varepsilon\sigma(\Delta z)}\tau_1 + T_\infty^4 + \frac{h}{\varepsilon\sigma}T_\infty + \frac{\varepsilon}{\sigma}(q'' + q_{fl}'') - \frac{k}{\varepsilon\sigma}\rho H_g \upsilon\right] = 0, \quad (19)$$

and

$$T_{0,j}^4 + \left[\frac{h}{\varepsilon\sigma} + \frac{k}{\varepsilon\sigma(\Delta z)}\right]T_{0,j} - \left[\frac{k}{\varepsilon\sigma(\Delta z)}T_{1,j} + T_\infty^4 + \frac{h}{\varepsilon\sigma}T_\infty + \frac{\varepsilon}{\sigma}(q'' + q_{fl}'') - \frac{k}{\varepsilon\sigma}\rho H_g \upsilon\right] = 0. \quad (20)$$

respectively. Similarly, for i=N, the values of τ_{N+1} and $T_{N+1,j}$ are taken as the positive real roots of the corresponding boundary condition, Eq. (4), expressed such that

$$\tau_{N+1}^4 + \left(\frac{h + k/\Delta z}{\varepsilon\sigma}\right)\tau_{N+1} - \left(\frac{k/\Delta z}{\varepsilon\sigma}\right)\tau_N - \left(\frac{h}{\varepsilon\sigma}\right)T_\infty - T_\infty^4 = 0, \quad (21)$$

and

$$T_{N+1,j}^4 + \left(\frac{h + k/\Delta z}{\varepsilon\sigma}\right)T_{N+1,j} - \left(\frac{k/\Delta z}{\varepsilon\sigma}\right)T_{N,j} - \left(\frac{h}{\varepsilon\sigma}\right)T_\infty - T_\infty^4 = 0. \quad (22)$$

The convergence criterion is set as relative error less than 10^{-5}.

2. Experimental Setup

The cylinder wall consists of an inner aluminum liner and seven sub-laminates of carbon/epoxy (Fig. 2). Each hoop (90°) and helical (20−12°) sub-laminate consists of many laminas. The carbon fiber sheets (T700SC-24000-50C, Toray Industries. Inc) were prepared using a hoop-and-helical-winding method on a mandrel. Poly-

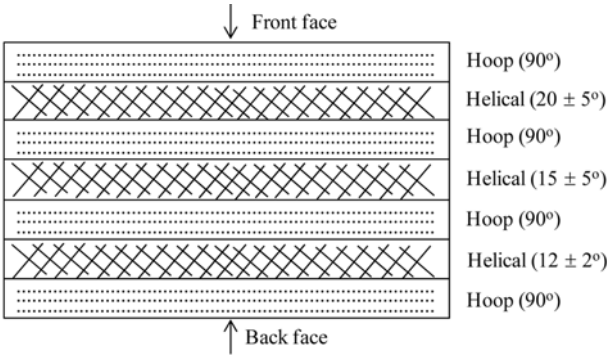

Fig. 2. Cross-sectional view of the pressure vessel showing the stacking sequence.

mer resin was made of a 100:32 mixture of epoxy (HPV-2000, AK Chemical) and hardner (Akamine-0230, AK Chemical). The blend was added to the woven carbon fiber sheet and then cured in a convection oven for 120 min (85 °C during the first 60 min and 120 °C during the remaining time). After baking, the sheet was tailored into a square: each side measuring 100 mm, with a thickness of 7.9 mm. In the specimen, the volume fractions of fiber and resin are 0.65 and 0.35, respectively. The instrumental set up is shown in Fig. 1(a). The specimen was then placed on the holder of a cone calorimeter (FESTEC®, Korea); see Fig. 1(a). Heat was added to only one side of the specimen (front face) at the setting values of 25, 40, 50, 60, and 75 kW/m^2. The components in the exhaust gas were examined with a gas purity analyzer (Servomex®4100, USA) and recorded by a data acquisition system (Agilent 34970A, USA). Thermocouples (K-type thermocouple, 1,523 K) were installed on both the front and back faces to measure the specimen's real-time temperatures, see Fig. 1(b).

The cone heater that burns methane as fuel is placed 60±1 mm above the front face of the specimen. The heat flux from the heater is measured by the heat flux meter (Medtherm®, USA). The temperature of the coolant in the heat flux meter is kept at 294 K by water circulation. The specimen is fixed to the holder (111 mm wide, 111 mm long, and 1.9 mm thick) which is initially at room temperature. The test is initiated by opening a shutter of the radiant heater. Before starting the test, the heater is warmed up for at least 30 min, which guarantees a stable radiation of heat. The temperature changes at the front and the back faces are measured by attaching the thermocouples at the faces, and recorded by the computer. The mass change of the specimen is measured by using the micro load cell (SMC, Japan), and recorded in the same way. The experiment with the cone calorimeter is performed in accordance with the guidelines by ISO 5660-1:2002 [20].

Laser flash method (NETZSCH, LFA 457, Germany) under Argon environment is used to analyze the thermal properties of the specimen such as density, heat capacity, and thermal conductivity. In the analysis, the thickness and the diameter of the sample are 1.753 mm and 12.7 mm, respectively. The measurement of the property is possible only at the temperature below 573 K because of smoke. The values above 573 K are estimated by the linear extrapolation of the acquired values at lower temperature.

RESULTS AND DISCUSSION

As shown in Fig. 3, the increase in temperature from 298 K to 573 K leads to the increase in the heat capacity of the specimen C_p from 1,076.75 to 1,485.25 J/kg K, which is around 38% rise. In the same range of temperature, the thermal conductivity k decreases from 0.77 to 0.53 W/m K, and the density ρ also decreases from 1,575 to 1,563 kg/m^3. The temperature dependency of the density is negligible when compared to the other properties. The thermal diffusivity, computed to thermal conductivity divided by the product of density and heat capacity, decreases by 50.3% as a result of temperature rise from 298 K to 573 K.

As a result of TGA tests for the specimen, thermal decomposition occurs when the weight loss exceeds around 5% of the original weight. The temperature during this time ranges from 575 K to 648 K. Therefore, the ignition temperature in this study was determined to

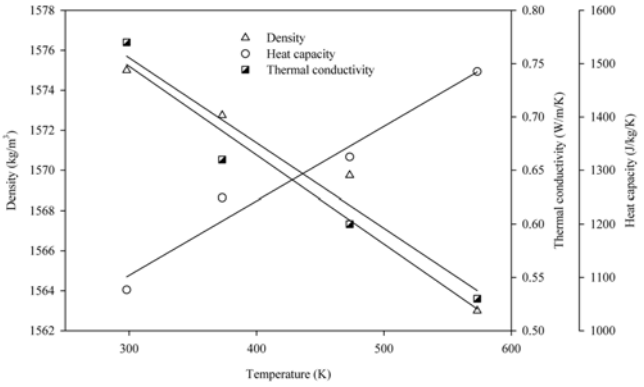

Fig. 3. Thermal properties test results using a laser flash method.

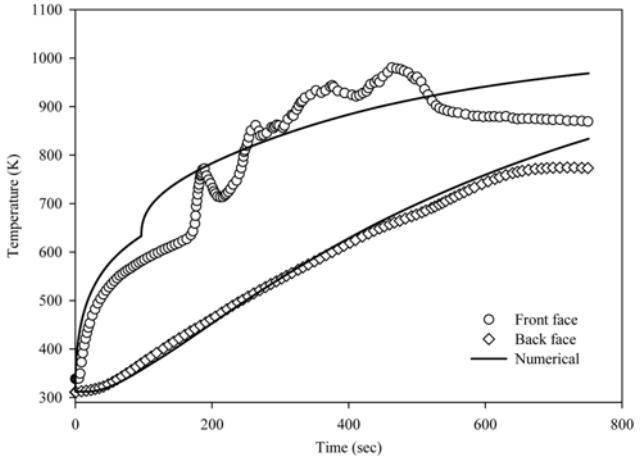

Fig. 4. Time-courses of temperatures on the front (circles) and back (diamonds) faces when heat flux of 50 kW/m^2 is applied. Solid lines denote the simulation results.

620 K. Because the thermal decomposition produces flammable volatile gas on a surface of a specimen, the accumulation of gas more than the minimum combustion level results in flames.

The temperatures on the front and the back faces of the specimen when a 50 kW/m^2 radiant heat flux is applied are shown in Fig. 4. In Fig. 4, the experimental measurements and the results of the numerical simulations are compared. The ignition time is defined as the time elapsed before the thermal decomposition begins or the temperature of the front face reaches the ignition temperature, i.e., T_{ig} (=620 K). This is calculated to 96 seconds in the numerical simulations. In the experimental portion of the study, however, temperature fluctuation occurs after 163 seconds due to the flame heat flux. The delay is caused by the effect of the burning flame heat flux on the surface and by the fact that temperature becomes significant only after the fire is fully developed [21] while in computation its immediate effect is assumed. The exposure to heat of the front face forms an initial temperature gradient across the thickness of the composite material, and, due to its continuous exposure to heat, the magnitude of the gradient becomes gradually reduced.

Unlike the temperature profile of the front face, the change in the temperature at the back face is not sharp (Fig. 4). This implies that the composite material acts as a thermal insulator. One point to note is that the model prediction for the back face is very close to

the temperature obtained by the experiment, while the simulation can predict merely the trend of the temperature at the front face due to the flame. According to the good agreement at the back face, we can confirm the validity of the model developed. It is also important to mention the effect of the liner at the back face. The liner used in the specimen is 3 mm thick and made of Al 6061 T6 (Type III), which has relatively high thermal conductivity and low heat capacity. Therefore, the existence of the liner in this heat transfer problem does not make significant difference in the analysis, and the temperature of the liner can be considered same as that of the back face. If the liner is made of high density polyethylene (HDPE, Type IV), we do not ignore the existence of liner because of the low heat transfer property of HDPE.

The pyrolysis or the surface recession of CFRP significantly occurs when the temperature at the surface rises above the ignition temperature. The heat transfer mechanism that the CFRP layer undergoes depends highly on whether the pyrolysis happens or not. Thus, the whole simulation has been conducted by putting two sub-simulations together. The one sub-simulation is to describe heat transfer in a constant-thickness CFRP layer before the ignition takes place with the at-rest initial condition. The other is for the moving boundary heat transfer problem in the CFRP layer after the ignition occurs. Note that the final values of the former simulation are put into the latter as initial conditions.

By the way, the flame heat flux is considered in the second simulation. A certain portion of heat released as a result of combustion of the resin contributes back to the temperature rise of the CFRP layer. The amount of heat released per unit mass of resin can be calculated by consulting the heat of formation. However, there is no reliable method developed to measure the portion of heat that is transferred back into the resin. Instead, there are some prior works that can be used as the guideline for this issue: Rhodes and Quintiere obtained a constant flame heat flux of 37 kW/m^2 when the radiant heat flux in the range up to 70 kW/m^2 is applied to PMMA surface [22]; Wasan et al. set the maximum flame heat flux to 10 kW/m^2 and let it exponentially decrease as time elapsed [23].

We assumed that the portion of the flame heat flux that transferred to the CFRP layer be the same as that of the radiant heat flux. To examine this assumption, five sets of tests were performed with different incident heat fluxes of 25, 40, 50, 60 and 75 kW/m^2. Each heat flux yields the characteristic burning flame heat flux and the ratio of the final to the initial masses of the specimens. In Fig. 5, the flame heat flux is plotted as a function of the final mass in the percentage of the initial value. According to the results of the experiment with the cone calorimeter, the portion of the radiant heat flux is a decreasing function of the radiant heat flux itself. Therefore, using the same rate of the decrease, the estimated flame heat fluxes that are used into simulations are 35, 24, 20, 10 and 2 kW/m^2 for the radiant heat fluxes of 25, 40, 50, 60 and 75 kW/m^2.

From Fig. 5, it can be said that the large incident heat flux results from a small burning flame heat flux, and the ratio of the final to the initial masses. In addition, a large incident heat flux will reduce the temperature difference between the front and the back faces of the composite. In other words, the time elapsed before the inner epoxy resin reaches its thermal decomposition temperature (T_{ig}) is reduced by a large incident heat flux, while the amount of flammable volatile gas required for the ignition increases. These changes lead to a large consumption of resin.

In Fig. 6, the results of comparisons between the experimental and the simulations for the change in the mass of the specimen normalized by the initial mass due to the applied heat flux over time are drawn. The model-based estimation is performed by plugging the temperature at the first computational node into Eq. (1) because decomposition is assumed, in this study, to take place only at the surface. As shown in Fig. 6, the results of the simulations through the present model accurately predict the experimental data. Yet, there is a 284-second discrepancy between the simulations and the experiments in terms of the point in time at which the mass loss begins to occur. This is because the model assumes that ignition begins only when the surface temperature reaches the ignition temperature while its decomposition, although it may be slow, in an actual situation occurs as soon as the sample is exposed to heat [24].

The surface recession depths are plotted in Fig. 7. These were

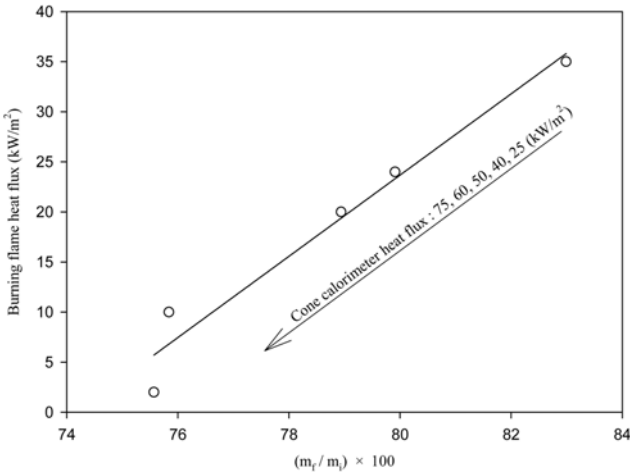

Fig. 5. Relation between burning heat flux (one-dimensional model-based simulations) and ratio of final to initial masses (from cone calorimeter experiments) with various incident heat fluxes (25, 40, 50, 60, and 75 kW/m^2).

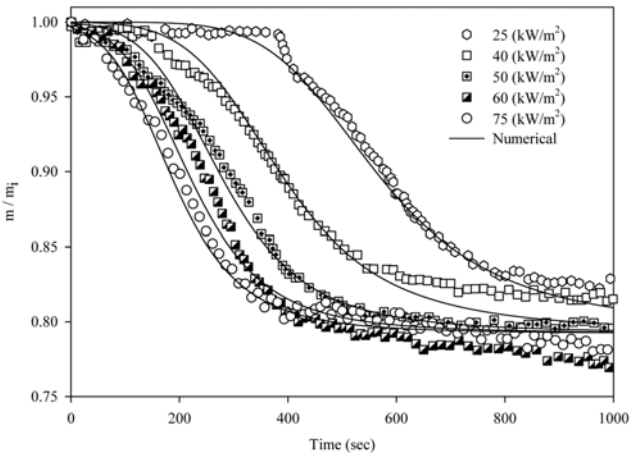

Fig. 6. Time courses of ratio of RRC to initial mass with various incident heat fluxes (25, 40, 50, 60, and 75 kW/m^2): symbols come from cone calorimeter experiments, and lines are one-dimensional model-based simulation results.

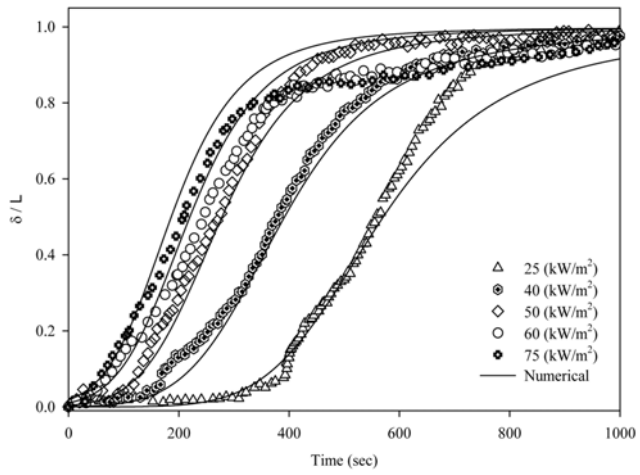

Fig. 7. Time courses of surface recession depths with various incident heat fluxes (25, 40, 50, 60, and 75 kW/m^2): symbols come from cone calorimeter experiments, and lines are one-dimensional model-based simulation results.

measured using the cone calorimeter and calculated according to the model. When heat is applied at 25 kW/m^2, the model accurately predicts the experimental data until 50% of the initial resin is degraded. In the case of a 40-50 kW/m^2 heating rate, the prediction is in accordance with the experimentally measured data for the entire mass range. There are discrepancies between the prediction and the measurement when 60-75 kW/m^2 of heating rate is applied. The difference is caused by the char formation under a high heating rate. The char formed as a result of the polymer resin decomposition can inhibit heat flux (this is also known as thermal barrier effect).

Fig. 8 shows the linear relation between the ratio of final to initial masses and the ratio of final to initial surface recession depths. The linear relation validates the hypothesis stating that the normalized surface recession depth can be indirectly estimated by measuring mass loss. As shown in Fig. 8, the data points in the range of 40-50 kW/m^2 are on a straight line. However, as heating continues, the data points show non-linear behavior (after approximately 80% of initial mass has been lost). Gibson et al. [12] in addressing this issue state that as the decomposition approaches completion, the thermal barrier effect brought about by the accumulated char in the composite material is magnified.

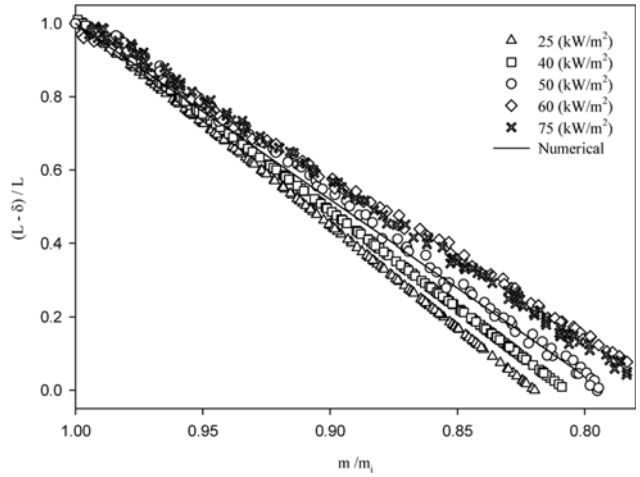

Fig. 8. Comparison of ratios: surface recession depth to initial thickness vs. RRC to initial mass.

CONCLUSIONS

The thermal decomposition of a composite cylinder wall has been tested to find the characteristics of the thermal resistance of a carbon-fiber-reinforced tank. A specimen was taken from a cylinder made of fiber-filament-wounded epoxy resin. The tests were conducted through computer simulation and experimental methods, and their results were subsequently compared. In the modeling stage, we employed the simplified one-dimensional heat transfer model due to a large radius of curvature of the tank. The thermal decomposition rate of polymer resin contained in the composite material is expressed by a one-step Arrhenius-type kinetics. To represent the extent of the resin disintegration, the surface recession depth was considered in the simulations, while the mass of the residual resin content was actually measured in the experiment. To compare the results of two approaches, the hypothesis was made that the ratio of thickness to its initial value is same as the ratio of mass to its initial value. The relevant cone-calorimeter experiments were also conducted to prove this hypothesis. Finally, we obtained the simulation results that can predict the experimental data such as the surface recession rate and the temperatures at both surfaces.

NOMENCLATURE

A : overall pre-exponential factor [sec^{-1}]
a_s : specimen area [m^2]
C_p : heat capacity [J kg^{-1} K^{-1}]
C_{p0} : heat capacity at [J kg^{-1} K^{-1}]
E_a : activation energy [J mol^{-1}]
h : convective heat transfer coefficient [W m^{-2} K^{-1}]
H_g : heat of decomposition [J kg^{-1}]
k : thermal conductivity [W m^{-1} K^{-1}]
L : initial thickness of the specimen [m]
m : mass [kg]
n : reaction order [-]
q″ : radiant heat flux of cone calorimeter [Wm^{-2}]
q''_{fl} : burning flame heat flux [Wm^{-2}]
R : universal gas constant [Jmol^{-1} K^{-1}]
t : time [sec]
T_{ig} : ignition temperature [K]
T_p : pyrolysis temperature [K]

Greek Letters

δ : surface recession depth [m]
ε : emmisivity [-]
ρ : density [kg m^{-3}]
σ : Stefan-Boltzmann constant [Wm^{-2}]
τ : dummy variable
υ : surface recession rate [m·sec^{-1}]

Superscripts

″ : unit area

Subscripts

f : final
fl : flame
g : gas
i : initial
ig : ignition
L : back face
p : pyrolysis
r : resin
s : surface or specimen
∞ : ambient

REFERENCES

1. J. C. Thesken, P. L. N. Murthy, S. L. Phoenix, N. Greene, J. L. Palko, J. Eldridge, J. Sutter, R. Saulsberry and H. Beeson, NASA/TM-2009-215684 (2009).
2. G. A. Pering, P. V. Farrel and G. S. Springer, *J. Comp. Mater.*, **14**, 54 (1980).
3. G. S. Springer, *J. Reinforced Plastics and Compo.*, **3**, 85 (1984).
4. J. B. Henderson, J. A. Wiebelt and M. R. Tant, *J. Comp. Mater.*, **19**, 579 (1985).
5. J. K. Chen, C. T. Sun and C. I. Chang, *J. Comp. Mater.*, **19**, 408 (1985).
6. N. Dodds, A. G. Gibson, D. Dewhurst and J. M. Davis, *Compo.: Part A*, **31**, 689 (2000).
7. P. Krysl, W. T. Ramroth, L. K. Stewart and R. J. Asaro, *Int. J. Numer. Meth. Eng.*, **61**, 49 (2004).
8. J. Trelles and B. Y. Lattimer, *Fire Mater.*, **31**, 147 (2007).
9. Y. Bai, T. Vallée and T. Keller, *Compo. Sci. Technol.*, **68**, 47 (2008).
10. Y. M. Sohn, S. W. Baek and T. Kashiwagi, *Combust. Sci. Technol.*, **145**, 83 (1999).
11. A. P. Mouritz and Z. Mathys, *Compo. Sci. Technol.*, **61**, 475 (2001).
12. A. G. Gibson, P. N. H. Wright, Y. S. Wu, A. P. Mouritz, Z. Mathys and C. P. Gardiner, *Plastics, Rubber and Compo.*, **32**, 81 (2003).
13. C. P Gardiner, Z. Mathys and A. P. Mouritz, *Marin Struct.*, **17**, 53 (2004).
14. P. J. Burchill, Z. Mathys and C. P. Gardiner, *Fire Mater.*, **29**, 249 (2005).
15. C. A. Griffis, R. A. Masumura and C. I. Chang, *J. Comp. Mater.*, **15**, 427 (1981).
16. M. Kindelan and A. Liñán, *Acta Astronaut.*, **5**, 1199 (1978).
17. T. Keller, C. Tracy and A. Zhou, *Compo.: Part A*, **37**, 1286 (2006).
18. J. E. J. Staggs, *Polym. Degrad. Stabil.*, **82**, 297 (2003).
19. R. E. Lyon and J. G. Quintiere, *Combust. Flame*, **151**, 551 (2007).
20. ISO 5660-1 (2002).
21. B. Schartel and T. R. Hull, *Fire Mater.*, **31**, 327 (2007).
22. B. T. Rhodes and J. G. Quintiere, *Fire Safety J.*, **26**, 221 (1996).
23. S. R. Wasan, P. Rauwoens, J. Vierendeel and B. Merci, *Fire Mater.*, **35**, 261 (2011).
24. F. JIa, E. R. Galea and M. K. Patel, *Fire Mater.*, **23**, 71 (1999).